Energy and AI 26 (2026) 100923

Contents lists available at ScienceDirect

Energy and AI

journal homepage: www.elsevier.com/locate/egyai

Homogenized modeling of coupled flow–heat transfer in plate heat exchangers with variable channels and flow configurations ☆

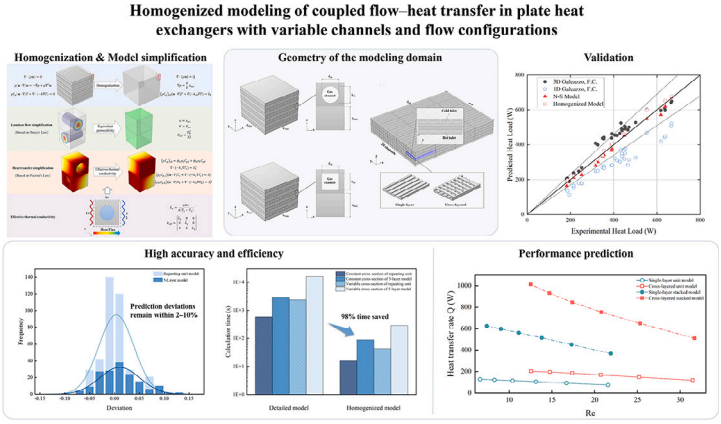
Xiaolu Wang [a], Shuang Zhao [a], Jan Van herle [b], Oscar Furst [c], Olaf Deutschmann [c], Xing-Yuan Miao [d], Yumeng Zhang [a], Umberto Desideri [e], Ligang Wang [a,f,*], Yongping Yang [f]

[a] Beijing Laboratory of New Energy Storage Technology, North China Electric Power University, Beijing, 102206, China
[b] Group of Energy Materials, Swiss Federal Institute of Technology in Lausanne, Sion, 1950, Switzerland
[c] Karlsruhe Institute of Technology, Baden-Württemberg, 76131, Germany
[d] Department of Wind and Energy Systems, Technical University of Denmark, Roskilde, 4000, Denmark
[e] Department of Energy, Systems, Territory and Constructions Engineering, University of Pisa, Pisa, 56126, Italy
[f] Center of Hydrogen Energy and Low Carbon, Lanzhou University, Lanzhou, 730000, China

HIGHLIGHTS

- A homogenized porous-medium model is proposed for coupled thermo-fluid transport.
- The model is applicable to variable cross-section and cross-layered channel configurations.
- Prediction deviations remain within 2%–10% under different operating conditions.
- Computational time is reduced by about 97% compared to Navier–Stokes models.

GRAPHICAL ABSTRACT



ARTICLE INFO

Keywords:
Compact plate heat exchangers
Porous media
Homogenization

ABSTRACT

Plate heat exchangers are widely used in energy conversion systems due to their high efficiency and compact structure. However, their complex stacked geometries and strong coupling between flow and heat transfer make high-fidelity Navier–Stokes equation-based simulations computationally expensive, while existing porous media modeling approaches often focus on either flow or heat transfer of standardized regular structures. To address these limitations, a fully coupled three-dimensional homogenized modeling approach is developed for design and simulation of plate heat exchangers with complex cross-section/layered channels, enabling the simultaneous homogenization of coupled flow and heat transfer while retaining anisotropic transport properties, interlayer differences, and macroscopic characteristics within the full 3D domain. The approach employs an equivalent anisotropic porous medium representing detailed channel structures, with the flow field described using Darcy's law and heat transfer represented by an equivalent thermal conductivity tensor for efficient simulation of the coupled process. The approach is validated using five-layer stacked structures. The results show that the model performs well across geometries and conditions, with deviations within

☆ This article is part of a Special issue entitled: 'AI in flow & heat transfer' published in Energy and AI.

* Correspondence to: North China Electric Power University, China.
E-mail address: ligang.wang@ncepu.edu.cn (L. Wang).

https://doi.org/10.1016/j.egyai.2026.100923
Received 18 August 2026; Received in revised form 17 September 2026; Accepted 27 September 2026
Available online 10 October 2026
2666-5468/© 2026 The Authors. Published by Elsevier Ltd. This is an open access article under the CC BY-NC-ND license (http://creativecommons.org/licenses/by-nc-nd/4.0/).

2%/10% under moderate/large temperature differences and 5% for variable cross-section and cross-layered configurations. The computational cost is reduced by more than 97% compared with the Navier–Stokes model. The model further identifies that the cross-layered configuration can enhance heat transfer by 50%–60%. The methodology is expected to support both heat exchanger manufacturers and system designers by reducing computational effort and dependence on detailed proprietary information, while facilitating more effective interaction between manufacturers and users.

1. Introduction

Plate heat exchangers (PHEs) are widely applied in aerospace, automotive, and gas turbine systems due to their high efficiency and compact design [1]. Typical types include plate, plate-fin, spiral, printed circuit, and microchannel heat exchangers [2]. These devices consist of densely arranged heat transfer surfaces with integrated flow distribution structures, which provide high thermal performance, compactness, and reliability.

Although compact heat exchangers have been widely standardized in terms of structure and application, in practical applications, manufacturers and system users aim to further reduce material consumption and device size while improving design flexibility for unconventional channel geometries and emerging operating conditions [3,4]. Accurate and efficient numerical approaches thus remain important for the design and optimization of such compact heat exchangers; however, high-fidelity computational fluid dynamics (CFD) models often involve tens of millions of computational cells and require substantial computational resources [5]. This computational cost mainly results from complex geometries, which introduce numerous fluid–solid interfaces, stringent mesh requirements, and strongly coupled governing equations. In addition, full Navier–Stokes simulations require detailed knowledge of local flow and heat transfer characteristics and are difficult to validate experimentally except in specific cases or by manufacturers with access to detailed measurements.

From the users' perspective, detailed prediction of heat transfer performance also requires considerable human and computational effort. In practical engineering applications, the sizing and selection of heat exchangers are often based on lumped parameters provided by manufacturers, which simplifies the design process but limits predictive accuracy and flexibility for new configurations. Therefore, there is a strong need for modeling approaches that provide higher accuracy than lumped parameter models while requiring substantially lower computational and human effort than full Navier–Stokes CFD simulations.

Existing CFD model simplification strategies can generally be classified into two categories: algorithm simplification and geometric simplification. Algorithm simplification reduces computational cost by simplifying governing equations or introducing empirical correlations to approximate transport processes, whereas geometric simplification reduces model complexity by neglecting secondary components such as headers or flow distributors.

Algorithm simplification approaches aim to preserve macroscopic thermo-fluid behavior while reducing computational complexity. One common strategy is equation-level simplification. This approach derives effective permeability through asymptotic expansion or approximates channel flow using Darcy's law with equivalent or spatially varying permeability [6,7]. These methods significantly reduce computational cost compared with full Navier–Stokes models. The inclusion of resistance terms enables the prediction of pressure losses and supports extension to multi-channel configurations with acceptable errors [8]. Another strategy is micro-volume transport modeling. This approach discretizes the system into control volumes to establish a cross-scale framework that links local transport processes to macroscopic performance. It has been validated for heat exchangers and shows good agreement with experimental flow and temperature distributions [9]. In addition, algorithm simplification can be applied to heat transfer modeling through equivalent parameter fitting. In this approach, effective material properties (e.g., Young's modulus, Poisson's ratio, and shear modulus) are expressed as functions of temperature. This method reduces thermal deformation errors to below 4% and improves computational efficiency by more than one order of magnitude [10,11].

Data-driven reduced-order modeling provides another approach to accelerating heat exchanger design and analysis. Yang et al. [12] combined snapshot proper orthogonal decomposition with neural-network regression to rapidly generate optimized microchannel configurations and predict the associated temperature, velocity, and pressure fields, achieving prediction errors below 2% and a computational acceleration exceeding 7200 times.

As a representative means of geometric simplification, porous media models [13] are widely applied in numerical simulations of heat exchangers, particularly for fluid flow in tube bundles, to predict temperature and pressure drop. Previous studies have applied these models to various configurations [14–16]. For example, in 3D finned tube heat exchangers, porous media models achieve pressure drop errors below approximately 10% [17]. Zeng et al. developed a porous-media-based, tube-level 3D method that combines distributed flow-resistance and energy-exchange source terms with a two-fluid model [18]. Applied to a full-scale 4474-tube steam generator, the method predicted individual-tube flow distribution and spatially varying thermal-hydraulic characteristics without resolving the complete tube-bundle geometry [19]. In tube bundle regions with two-phase flow and boiling heat transfer, these models simplify the simulation while maintaining pressure drop and temperature errors of approximately 13% [20]. In plate-fin heat exchangers, porous media models are used to analyze flow and heat transfer characteristics with high computational efficiency [21–23]. In low-temperature plate-fin heat exchangers, 3D transient and steady-state simulations are performed by combining empirical correlations for heat transfer and pressure drop in fin materials [24,25]. These approaches achieve average temperature distribution errors of less than 1 K while reducing grid count and computational cost, thereby enabling the simulation of complex multi-layer heat exchanger structures.

Porous media modeling can be extended through homogenization, in which heterogeneous structures are represented as equivalent homogeneous media with anisotropic effective properties. Under the assumption of periodicity, detailed geometrical features are replaced by macroscopic transport parameters. This treatment enables efficient simulation of coupled heat and mass transfer without resolving micro-scale structures. The approach is widely applied in porous and composite systems where full-resolution modeling is computationally prohibitive. It has also been applied to solid oxide fuel cell stacks and multi-stack modules to predict thermo-fluid behavior [26–29].

Most existing heat exchanger models focus on simplified calculations of individual flow or heat transfer processes [8,9,30]. The coupling between flow and heat transfer is often not fully considered [22–24]. Their effective parameters are commonly derived from empirical correlations, experimental data, or detailed simulations and may require recalibration for different geometries or operating conditions. Moreover, reduced-dimensional models have a limited ability to represent interlayer differences and local flow redistribution. These limitations motivate a physics-based three-dimensional framework that simultaneously homogenizes coupled flow and heat transfer using anisotropic and spatially varying transport properties. Such a framework is needed to efficiently represent macroscopic temperature and velocity fields and flow redistribution in variable-cross-section and cross-layered heat exchangers.

Therefore, there is a strong need to study new methods of designing compact heat exchangers, with higher accuracy than lumped-parameter

Nomenclature

A	Plane area	∇p	Pressure gradient in the flow direction
C_p	Specific heat capacity, J kg^{-1} K^{-1}	q_h	Heat flux, W m^{-2}
D_h	Hydraulic diameter, mm	Re	Reynolds number
d	Height, mm	S_T	Heat source term
f	Darcy friction factor	T	Temperature, K
K	Permeability	u_{av}	Average flow rate of the pore fluid, m^{-1}
k	Thermal conductivity, W m^{-1} K^{-1}	w	Width, mm
p	Pressure, Pa	z	Length, mm
Greek symbols			
Ω	Repeating unit volume	ρ	Density, kg m^{-3}
Subscripts			
c	Cold	out	Outlet
ch	Channel	PHE	Plate heat exchanger
h	Hot	s	Solid
in	Inlet		

models and with lower human and computational effort than full Navier–Stokes CFD models. This paper aims to address this challenge with a novel methodology satisfying both needs, by developing a homogenized modeling approach for fully coupled thermo-fluid behavior in PHEs. The heterogeneous structure is represented as an equivalent anisotropic porous medium, where the flow field is described using Darcy's law, and heat transfer is modeled using an effective thermal conductivity tensor. The method is applied to both repeating unit and multi-layer stacked configurations with constant and variable cross-section channels, and is validated against fully coupled detailed simulations under different thermal and geometric conditions. The proposed approach entails high accuracy and simplified applicability to different types of heat exchangers with limited use of computational resources and access to confidential information from manufacturers, and increases the interaction of manufacturers with users and system designers.

2. Homogenization of heterogeneous stacked structures

As shown in Fig. 1, the homogenization method [31] is used to simplify plate heat exchangers with multiple flow channels. The complex stacked structure is represented as an equivalent porous medium with simplified geometry, which enables efficient simulation of the overall thermo-fluid behavior. By solving the temperature, velocity, and pressure fields within the porous region, the performance of the stacked structure is predicted with reduced computational cost. In this framework, solid plates and fluid channels are treated as the matrix and pore phases of the porous medium, respectively.

To approximate fully developed laminar flow, Darcy's law is reformulated based on its analogy with the Darcy–Weisbach equation. A spatially varying permeability is introduced to reproduce the velocity profile obtained from the Darcy–Weisbach formulation. For heat transfer, an equivalent anisotropic thermal conductivity tensor is used to represent the effective transport properties in the homogenized domain.

2.1. Numerical methods for the calculation of homogenization parameters

Each component exhibits distinct physical properties. Therefore, the effective homogenized parameters are calculated by treating the heterogeneous structure as a representative unit. In this work, the volume-averaging method is used to obtain the effective parameters.

Taking the effective thermal conductivity as an example, as shown in Fig. 1, Fourier's law is applied to determine the heat flux. The effective thermal conductivity $\bar{k}_x$ along the x direction is calculated as follows:

$$\bar{k}_x = \frac{q\Delta x}{T_1 - T_2} \tag{1}$$

where q is the heat flux density, T_1 and T_2 are the temperatures at the left and right boundaries, and Δx is the distance between the two temperature boundaries. The effective thermal conductivities along the y and z directions are calculated using the same approach. The anisotropic thermal conductivity tensor is then expressed as:

$$\bar{k} = \begin{bmatrix} \bar{k}_x & 0 & 0 \\ 0 & \bar{k}_y & 0 \\ 0 & 0 & \bar{k}_z \end{bmatrix} \tag{2}$$

2.2. Approximation of laminar flow

Darcy's law is a linear empirical relation that describes the relationship between fluid velocity and pressure gradient in porous media, and allows efficient and numerically stable solutions. In this work, the similarity between Darcy's law and the Darcy–Weisbach equation is used to derive a modified form that represents laminar channel flow. For laminar flow in the channel with Reynolds number $Re_{air} < 2300$, the flow field is described by the Navier–Stokes equations:

$$\nabla \cdot (\rho \mathbf{u}) = 0 \tag{3}$$

$$\rho (\mathbf{u} \cdot \nabla) \mathbf{u} = -\nabla p + \mu \nabla^2 \mathbf{u} \tag{4}$$

where ρ is the density, $\mathbf{u}$ is the velocity vector, p is the pressure, and μ is the dynamic viscosity.

For laminar flow, Darcy's law is applied to describe the relationship between pressure gradient and average velocity in porous media [31]:

$$\nabla p = \frac{\mu}{K} u_{avg} \tag{5}$$

where u_{avg} is the average fluid velocity and K is the permeability. The permeability is determined by relating Darcy's law to the Darcy–Weisbach equation.

The Darcy–Weisbach equation describes the pressure drop in a channel as a function of fluid properties and average velocity:

$$\nabla p = f \frac{\rho}{2} \frac{{u_{avg}}^2}{D_h} \tag{6}$$

where D_h is the hydraulic diameter and f is the friction factor. For laminar flow, the friction factor is given by:

$$f = \frac{4 g_c}{Re} \tag{7}$$

and the Reynolds number is defined as:

$$Re = \frac{\rho u_{avg} D_h}{\mu} \tag{8}$$

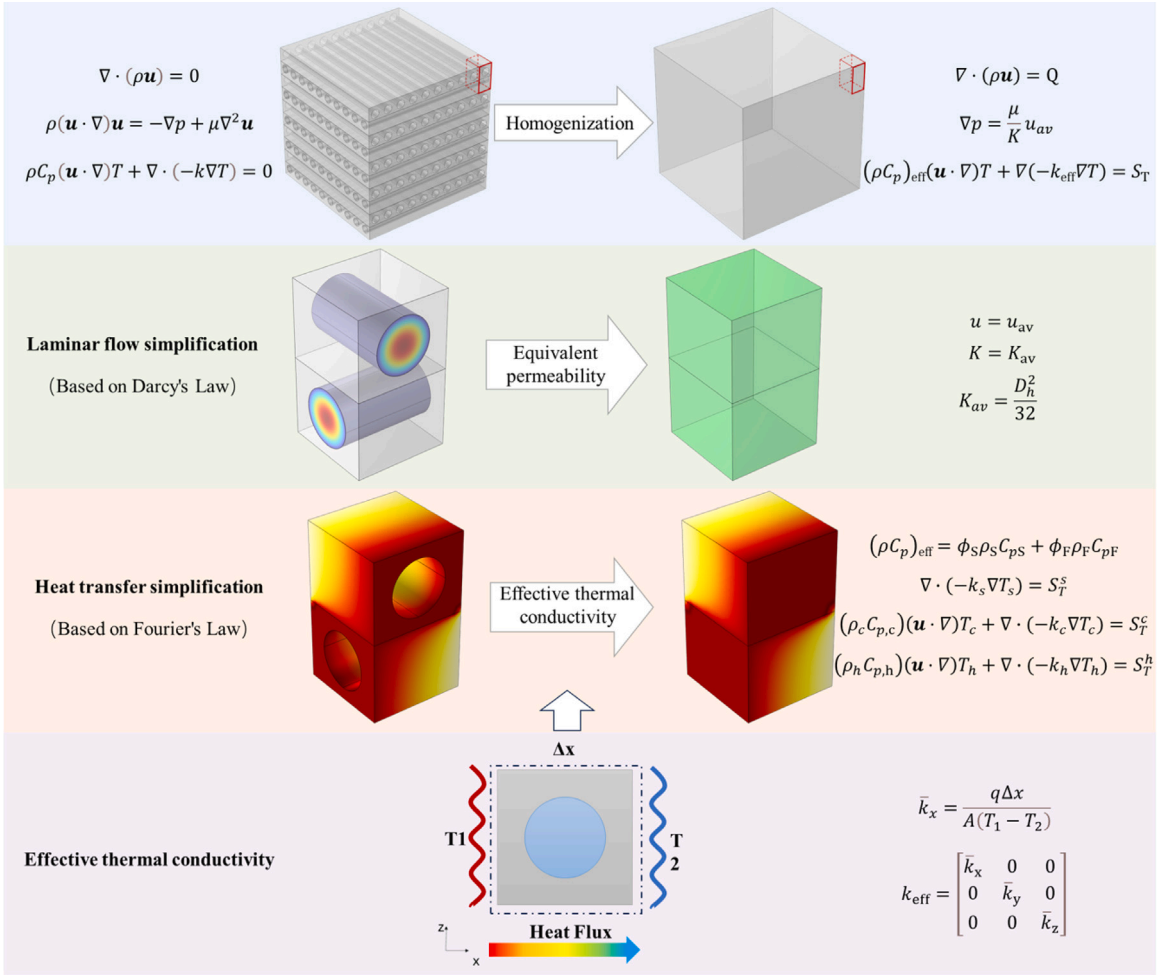


Fig. 1. Schematic illustration of the homogenization modeling approach.

Substituting Eqs. (7) and (8) into Eq. (6) gives:

$$\nabla p = \frac{\mu}{\frac{{D_h}^2}{2g_c}} u_{avg} \tag{9}$$

By comparing Eq. (9) with Eq. (5), the effective permeability in the flow direction is obtained as:

$$K_{av} = \frac{{D_h}^2}{2g_c} \tag{10}$$

where g_c is a correction factor related to the channel geometry. For circular channels, $g_c = 16$. For square channels, g_c is given by [32]:

$$g_c = 24\left(1 - 1.3553g_a + 1.9467{g_a}^2 - 1.7012{g_a}^3 + 0.9564{g_a}^4 - 0.2537{g_a}^5\right) \tag{11}$$

$$g_a = \min\left(\frac{w_{ch}}{z_{ch}}, \frac{z_{ch}}{w_{ch}}\right) \tag{12}$$

Under the fully developed laminar-flow assumption, Eq. (10) indicates that the equivalent permeability is determined by the local hydraulic diameter and cross-sectional shape and does not explicitly depend on the Reynolds number. Variations in the Reynolds number affect the pressure gradient and average velocity through the governing equations but do not alter the geometry-based permeability. This formulation is applicable to the viscous-dominated laminar regime considered in this study. At higher Reynolds numbers, where inertial effects, flow separation, or secondary flows become significant, an additional correction, such as the Darcy–Forchheimer term, may be required.

For the channel geometry considered here, the permeability is assigned only along the principal flow direction, while the permeability components in the two orthogonal directions are set to zero. This anisotropic representation constrains the fluid to flow along the channel direction and assumes no transverse flow or fluid exchange between adjacent channels.

2.3. Simplification of heat transfer model

The energy conservation equation is expressed as:

$$\rho C_p (\mathbf{u} \cdot \nabla) T + \nabla \cdot (-k\nabla T) = S_T \tag{13}$$

where T is the temperature, ρ is the density, C_p is the specific heat capacity, k is the thermal conductivity, and S_T is the heat source term. In the homogenized model, separate temperature variables are defined for different regions, including T_s, T_c, and T_h for the solid, cold fluid, and hot fluid, respectively. These variables are coupled through convective heat transfer to describe energy exchange between the regions:

$$\nabla \cdot (-k_s \nabla T_s) = S_T^s \tag{14}$$

$$\rho_c C_{p,c} (\mathbf{u} \cdot \nabla) T_c + \nabla \cdot (-k_c \nabla T_c) = S_T^c \tag{15}$$

$$\rho_h C_{p,h} (\mathbf{u} \cdot \nabla) T_h + \nabla \cdot (-k_h \nabla T_h) = S_T^h \tag{16}$$

where k_s is the equivalent anisotropic thermal conductivity of the solid phase, and k_c and k_h are the thermal conductivities of the cold and hot fluids, respectively. Through homogenization, these temperature

Table 1
Governing equations of flow and heat transfer.

Physical field	Equation	Coupling parameters
Mass	$\nabla \cdot (\rho \mathbf{u}) = Q$	$\rho(T)$, $\mathbf{u}$
Flow	$\rho(\mathbf{u} \cdot \nabla)\mathbf{u} = -\nabla p + \mu \nabla^2 \mathbf{u} + \rho \mathbf{g}$ $\nabla p = \frac{\mu}{K} u_{\mathrm{av}}$	$\rho(T)$, $\mu(T)$, $\mathbf{u}$ $\mu(T)$, u_{av}
Heat	$\nabla \cdot \left(-k_{\mathrm{solid}} \nabla T_{\mathrm{solid}}\right) = S_{\mathrm{T}}^{\mathrm{solid}}$ $\rho_{\mathrm{fluid}} C_{\mathrm{p,fluid}} (\mathbf{u} \cdot \nabla) T_{\mathrm{fluid}} + \nabla \cdot \left(-k_{\mathrm{fluid}} \nabla T_{\mathrm{fluid}}\right) = S_{\mathrm{T}}^{\mathrm{fluid}}$ $\left(\rho C_{\mathrm{p}}\right)_{\mathrm{eff}} (\mathbf{u} \cdot \nabla) T + \nabla \cdot (-k_{\mathrm{eff}} \nabla T) = S_{\mathrm{T}}$	T, $\mathbf{u}$

variables are defined at each point in the computational domain and energy exchange is represented by volumetric source terms.

The convective heat transfer between the solid and fluid phases depends on the surface area of the channel, the temperature difference, and the heat transfer coefficient. In the homogenized formulation, this process is represented by volumetric source terms S_{T}:

$$S_{\mathrm{T}}^{\mathrm{c}} = h \frac{A_{\mathrm{ch}}}{|\Omega|} \left(T_{\mathrm{s}} - T_{\mathrm{c}}\right) = \frac{Nuk_{\mathrm{c}}}{D_{\mathrm{h}}} \frac{A_{\mathrm{ch}}}{|\Omega|} \left(T_{\mathrm{s}} - T_{\mathrm{c}}\right) \tag{17}$$

$$S_{\mathrm{T}}^{\mathrm{h}} = h \frac{A_{\mathrm{ch}}}{|\Omega|} \left(T_{\mathrm{s}} - T_{\mathrm{h}}\right) = \frac{Nuk_{\mathrm{h}}}{D_{\mathrm{h}}} \frac{A_{\mathrm{ch}}}{|\Omega|} \left(T_{\mathrm{s}} - T_{\mathrm{h}}\right) \tag{18}$$

$$S_{\mathrm{T}}^{\mathrm{s}} = -S_{\mathrm{T}}^{\mathrm{c}} - S_{\mathrm{T}}^{\mathrm{h}} \tag{19}$$

where A_{ch} is the convective heat transfer area, Ω is the control volume, and h is the convective heat transfer coefficient, defined as:

$$h = \frac{Nu}{D_{\mathrm{h}}} k_{\mathrm{air}} \tag{20}$$

For hydrodynamically and thermally fully developed laminar flow under a uniform wall heat flux, the Nusselt number is independent of the Reynolds number for a given channel geometry. Under the conditions considered in this study, $Nu = 4.36$ for circular channels and $Nu = 3.61$ for square channels [33].

For heat conduction in the solid domain, the equivalent anisotropic thermal conductivity is calculated using Eq. (2). Thermal radiation is neglected for temperatures below 1400 K [34].

2.4. Coupling analysis of laminar flow and heat transfer equations

Thermo–fluid characteristics arise from the intrinsic coupling of flow dynamics and heat transfer processes. Within the established model, the governing equations are solved in a coupled manner, with thermophysical parameters updated across varying temperature conditions. Key interactive mechanisms consist of variations in density and viscosity, and convective mass and energy transport (see Table 1).

Temperature-dependent properties introduce coupling between the governing equations. The fluid density $\rho(T)$ affects the momentum equation through the buoyancy term $\rho\mathbf{g}$, which modifies the flow field. The dynamic viscosity $\mu(T)$ influences the velocity distribution and the associated transport processes. The velocity field $\mathbf{u}$ determines the convective term in the energy equation, which controls the temperature distribution. These interactions establish a two-way coupling between flow and heat transfer.

In the present study, the flow and heat transfer equations are solved simultaneously to capture the coupled behavior. The model considers laminar flow with temperature-dependent properties and neglects phase change and turbulence effects. Under these assumptions, the coupled formulation provides a consistent representation of thermo-fluid transport in the homogenized domain.

3. Case study description

3.1. Plate heat exchanger with parallel straight channels

The homogenized model is applied to two types of compact plate heat exchangers. As shown in Fig. 2(a)–(b), one configuration has a symmetric structure with circular channels on both the cold and hot sides. The other configuration has an asymmetric structure with circular channels on the cold side and square channels on the hot side. Both configurations adopt a multi-plate stacked structure. The plates are made of stainless steel, and air is used as the working fluid. The channels are arranged in a staggered configuration, with cold and hot streams flowing perpendicular to each other. The geometric parameters and material properties of the PHE are listed in Tables 2 and 3. The channel geometry influences both heat transfer performance and hydraulic characteristics [35–37]. The two heat exchangers are modeled using three configurations:

- Model 1, referred to as the full-geometry Navier–Stokes laminar flow single repeating unit model (NS-SRU), retains detailed geometrical features and solves the Navier–Stokes equations for fluid flow.
- Model 2, referred to as the Darcy's law single repeating unit model (DL-SRU), applies Darcy's law to simplify the flow field based on Model 1, thereby reducing computational cost.
- Model 3, referred to as the Darcy–Fourier homogenized repeating unit model (DL-FL-HRU), further simplifies the geometry by representing it as a porous medium. Heat transfer in the solid domain is modeled using an equivalent anisotropic thermal conductivity based on Fourier's law.

Table 2
Geometry parameters of the heat exchanger models.

Parameter	Value	Units	Description
w_{PHE}	100	mm	Width of the plate heat exchanger
d_{PHE}	100	mm	Height of the plate heat exchanger
z_{PHE}	8.4	mm	Length of the plate heat exchanger
r_{ch}	3	mm	Radius of the channel
w_{ch}	3	mm	Width of the channel
z_{ch}	3	mm	Length of the channel

Table 3
Material properties of the heat exchanger.

Parameter	Value	Units	Description
k_{s}	15	W m^{-1} K^{-1}	Thermal conductivity of the stainless steel
ρ_{s}	7800	kg m^{-3}	Density of the stainless steel
$C_{\mathrm{p,s}}$	420	J kg^{-1} K^{-1}	Heat capacity for stainless steel

The NS-SRU model is used as the reference solution. The accuracy of the DL-SRU and DL-FL-HRU models is evaluated by comparing temperature and velocity deviations relative to the NS-SRU model. The deviation is defined as the relative difference in cross-sectional averaged values.

The cross-sectional averaged values are evaluated using area-weighted averages over the corresponding flow cross section. The average temperature and velocity are defined as

$$\overline{T} = \frac{1}{A_f} \int_{A_f} T \, \mathrm{d}A, \tag{21}$$

$$\overline{u} = \frac{1}{A_f} \int_{A_f} |\boldsymbol{u}| \, \mathrm{d}A, \tag{22}$$

where A_f is the flow cross-sectional area, T is the local temperature, and $|\boldsymbol{u}|$ is the local velocity magnitude.

The boundary conditions of the plate heat exchanger are summarized in Table 4. At the inlet, pressure and temperature boundary conditions are specified. At the outlet, a pressure outlet condition is imposed, and the heat flux is set to zero. No-slip boundary conditions are applied at the walls, and all external surfaces are assumed to be thermally insulated.

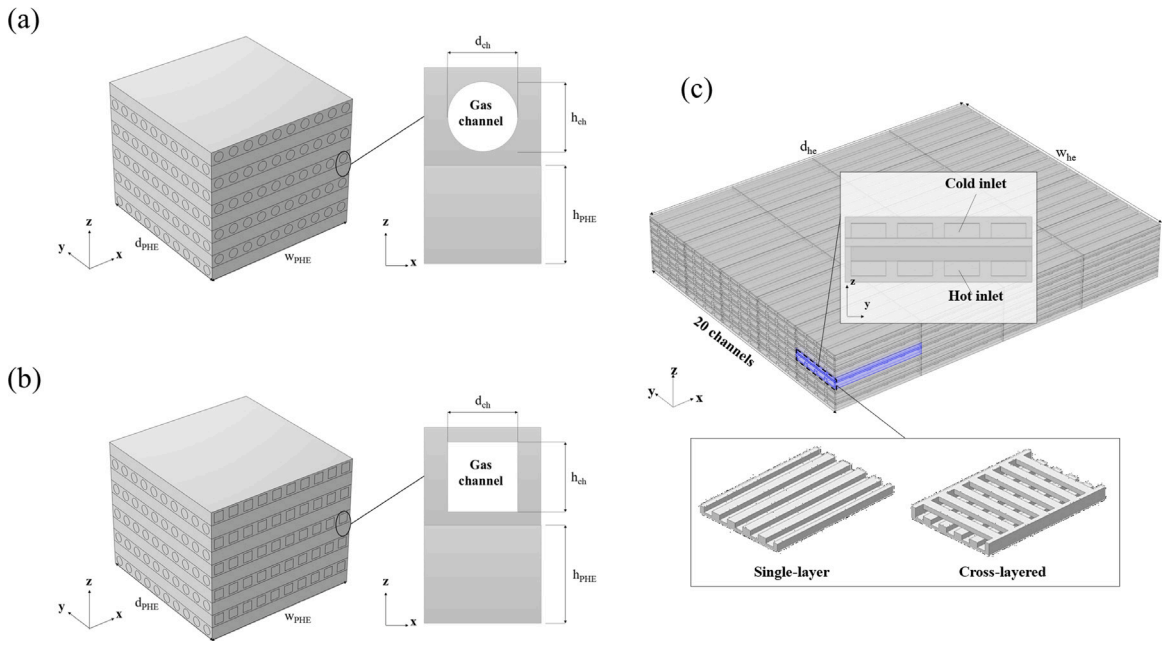


Fig. 2. Geometry of the modeling domain for a unit of crossflow heat exchanger SRU model and schematic diagram of parallel-flow plate heat exchanger with different arrangements.

Table 4
Boundary conditions of the heat exchanger models.

Parameter	Value	Units	Description
p_{in}	3	Pa	Inlet relative pressure
p_{out}	0	Pa	Outlet relative pressure
$T_{in,h}$	400	K	Inlet temperature for the hot flow
$T_{in,c}$	300	K	Inlet temperature for the cold flow

3.2. Plate heat exchanger with variable cross-section channels

Section 3.1 considers circular and square channels with constant cross sections along the flow direction. In practical applications, channel geometries in stacked structures are more complex and may vary along the flow direction. In addition to straight parallel channels separated by ribs, geometries such as wavy, trapezoidal, and staggered channels are used to enhance flow mixing and heat transfer [38–41]. In these configurations, the cross section varies along the flow direction. Therefore, a constant permeability is not sufficient to represent the flow field when replacing the Navier–Stokes equations.

To address this issue, a 3D model of a 20-channel parallel-flow plate heat exchanger is constructed, as shown in Fig. 2(c). Two representative channel configurations are considered: a straight channel formed by a single-layer arrangement of rectangular ribs, and a cross-layered channel formed by a staggered arrangement of ribs. These configurations are selected to assess the capability of the homogenized model to capture flow and heat transfer in channels with spatially varying geometry. The cross-layered configuration improves flow uniformity, reduces pressure drop, and increases fluid residence time, enhancing heat transfer performance. According to the modeling approach described in Section 3.1, both Navier–Stokes (N–S) and homogenized models are established for the two configurations. The geometric parameters and boundary conditions are summarized in Tables 5 and 6.

3.3. Model specifications

The governing equations for the NS-SRU, DL-SRU and DL-FL-HRU models are described in detail in Table 7. The assumptions used for the numerical calculation are as follows:

Table 5
Geometric parameters of the parallel-flow plate heat exchanger models.

Parameter	Value	Units	Description
w_C	57	mm	Width of the channel
z_C	67	mm	Height of the channel
d_C	1	mm	Length of the channel
w_{rib}	1	mm	Width of the rib
z_{rib}	0.5	mm	Height of the rib
w_{he}	44	mm	Weith of the heat exchanger
d_{he}	44	mm	Length of the heat exchanger

Table 6
Boundary conditions of the parallel-flow plate heat exchanger models.

Model	Boundary	Boundary conditions
Single-layer	Cold inlet	Air; 300 Pa (relative pressure); 300 K
	Hot inlet	H_2; 100 Pa (relative pressure); 500–1000 K
	Cold/Hot outlet	0 Pa (relative pressure); $-\mathbf{n}\cdot\mathbf{q}=0$
Cross-layered	Cold inlet	Air; 300 Pa (relative pressure); 300 K
	Hot inlet	H_2; 100 Pa (relative pressure); 500–1000 K
	Cold/Hot outlet	0 Pa (relative pressure); $-\mathbf{n}\cdot\mathbf{q}=0$

(1) The airflow is a compressible, steady-state, laminar flow;
(2) The inertial term is retained in the Navier–Stokes reference model but neglected in the Darcy-based models because the investigated flow conditions are within the viscous-dominated laminar regime;
(3) The thermophysical properties of the fluid are treated as temperature-dependent properties;
(4) Radiative heat transfer is excluded consistently from all models to isolate and evaluate the homogenized treatment of convection and conduction;
(5) Neglecting the viscous dissipation term in the energy equation;
(6) Local thermal non-equilibrium is assumed in the homogenized domains. Separate energy equations are solved for the fluid and solid phases, and their thermal interaction is represented by an interfacial heat-transfer source term.

COMSOL Multiphysics is used to build the models. Quadratic discretization is applied to the velocity field, and linear discretization

Table 7
Governing equations.

		Governing equation	
NS-SRU	Mass balance	$\nabla \cdot (\rho \mathbf{u}) = 0$	(4)
	Momentum balance	$\rho (\mathbf{u} \cdot \nabla) \mathbf{u} = -\nabla p + \mu \nabla^2 \mathbf{u} + \rho \mathbf{g}$	(5)
	Energy balance	$\rho C_p (\mathbf{u} \cdot \nabla) T + \nabla \cdot (-k \nabla T) = 0$	(23)
DL-SRU	Mass balance	$\nabla \cdot (\rho \mathbf{u}) = Q$	(24)
	Momentum balance	$\nabla p = \frac{\mu}{K} u_{av}$	(6)
	Energy balance	$\rho C_p (\mathbf{u} \cdot \nabla) T + \nabla \cdot (-k \nabla T) = 0$	(23)
DL-FL-HRU	Mass balance	$\nabla \cdot (\rho \mathbf{u}) = Q_m$	(25)
	Momentum balance	$\nabla p = \frac{\mu}{K} u_{av}$	(6)
	Energy balance	$(\rho C_p)_{eff} (\mathbf{u} \cdot \nabla) T + \nabla \cdot (-k_{eff} \nabla T) = S_T$	(26)

is applied to the pressure field. Heat transfer in both solid and fluid domains is discretized using linear elements. A segregated solver is employed, and the fluid flow and heat transfer variables are solved using the PARDISO solver to ensure stable convergence. Convergence was considered achieved when the relative residuals of all dependent variables decreased below 1×10^{-4}. All operating conditions reported in this study satisfied this criterion without residual divergence or persistent oscillation. All simulations were performed on a dual-socket Linux server equipped with two AMD EPYC™ 7H12 processors (64 cores each, 2.4 GHz; 128 cores in total), with 48 CPU cores allocated to each simulation.

For the fully resolved geometric model with parallel straight channels, unstructured tetrahedral meshes with local refinement near the channel walls are used, resulting in approximately 370,000 elements. In contrast, the homogenized model uses a coarser mesh with approximately 27,000 elements. Mesh independence verification is provided in the Supporting Information.

For the variable cross-section configurations, unstructured tetrahedral meshes with boundary layer refinement are employed to resolve the velocity field. Mesh convergence is evaluated using the cross-sectional average velocity as the indicator. As shown in the Supporting Information, when the total number of elements exceeds 8 million, the average velocity approaches a stable value, indicating mesh-independent solutions. Considering the balance between accuracy and computational cost, mesh sizes of 7.2 million and 8.21 million elements are adopted for the single-layer and cross-layered configurations, respectively.

3.4. Model validation

To validate the proposed model, the experimental data reported by Jorge A. W. Gut et al. and the 3D and one-dimensional CFD results from Flavio C. C. Galeazzo et al. are used for comparison [42–44]. Based on the geometric parameters of the plate heat exchangers in these studies, both parallel-flow and series-flow configurations are reconstructed. Corresponding N–S detailed models and homogenized models are established. The comparison results are presented in Fig. 3. The predicted heat load agrees with the experimental and numerical data within 15% over the range of operating conditions. This agreement indicates that the proposed model provides reliable predictions under different configurations and operating conditions.

4. Results and discussion

4.1. Constant cross-section plate heat exchangers

4.1.1. Comparison of circular-channel structure

The heat transfer and flow characteristics in a circular-channel cross-flow plate heat exchanger are evaluated using the NS-SRU, DL-SRU, and DL-FL-HRU models under two operating conditions with inlet temperatures of 300/400 K and 300/1000 K. The distributions of cross-sectional average velocity and temperature along the flow direction are shown in Fig. 4.

For the moderate temperature difference case, the flow remains laminar. The velocity decreases along the hot channel and increases along the cold channel due to density variation with temperature under a constant mass flow rate. The velocity change is limited due to the small temperature gradient. Both simplified models reproduce the NS-SRU results with small deviations. The maximum temperature deviation is within 6.0 K on the hot side and 3.5 K on the cold side, corresponding to relative errors within approximately ±2%, while the velocity deviation remains below 0.04 m/s. These results confirm that the simplified models provide accurate predictions under moderate temperature differences.

For the large temperature difference case, stronger coupling between flow and heat transfer is observed. The homogenized models capture the overall trends of velocity and temperature, although the deviation increases. For the DL-SRU model, the maximum temperature deviation reaches 23 K on the hot side and 18.3 K on the cold side. For the DL-FL-HRU model, the maximum deviation is 6.42% on the hot side and 9.03% on the cold side, with the largest discrepancy near the channel midpoint. The velocity deviation remains within ±3.0%. Despite the increased deviation, the accuracy remains acceptable for engineering applications.

To further assess the local behavior, transverse temperature and velocity profiles at axial positions of 0.01, 0.05, and 0.09 m are provided in the Supporting Information. The DL model captures the overall transverse temperature variation, although the discrepancy increases in the channel core. The velocity profiles reconstructed from the cross-sectional average DL velocities reproduce the parabolic distributions predicted by the NS-SRU model, whereas detailed near-wall features are not directly resolved by the homogenized model.

The increased deviation is attributed to the coupling between property variation with temperature and flow redistribution. Variations in density and viscosity modify flow resistance and reduce the volumetric flow rate under a fixed pressure drop, leading to lower velocities than in the moderate case. The error shows spatial dependence, with larger deviations in regions with strong temperature gradients, where the assumption of spatially uniform equivalent properties becomes less accurate.

Compared with the DL-SRU model, the homogenized model simplifies the geometry and introduces equivalent source terms and anisotropic thermal conductivity. This reduces local accuracy but preserves overall performance prediction.

4.1.2. Applicability of the homogenized model to geometry-varying channel structures

The applicability of the homogenized model to asymmetric channel structures is evaluated using a stacked configuration with a square cross section on the hot side and a circular cross section on the cold side. The inlet temperatures of the cold and hot fluids are 300 K and 1000 K, with corresponding inlet Reynolds numbers of 272 and 76. The cross-sectional average temperature and velocity distributions along the flow direction are compared in Fig. 5. The homogenized models capture the overall temperature evolution along the flow direction with good agreement. For the DL-SRU model, the maximum temperature deviation is 24 K with −4.2% on the hot side and 21 K with −4.3% on the cold side. For the DL-FL-HRU model, the maximum deviation is 42 K with 7.5% on the hot side and 32 K with 8.7% on the cold side. The velocity distributions also show consistent trends among the three models. The maximum velocity difference remains below 0.10 m/s, with relative deviations within ±9.5% for both streams. These results indicate that the homogenized models preserve the overall thermo-fluid behavior in geometry-varying channels.

The deviations are associated with the geometric characteristics of the flow channels. The simplification of the momentum equation based on Darcy's law depends on local flow resistance and velocity distribution. For square channels with an aspect ratio of 1:1, the friction factor can be predicted accurately using empirical correlations, with

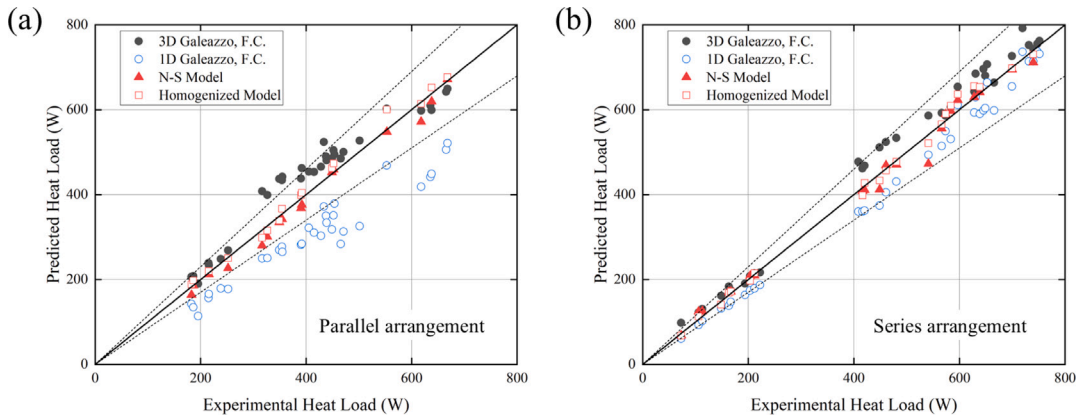


Fig. 3. Experimental and simulation results for heat load: (a) parallel arrangement; (b) series arrangement.

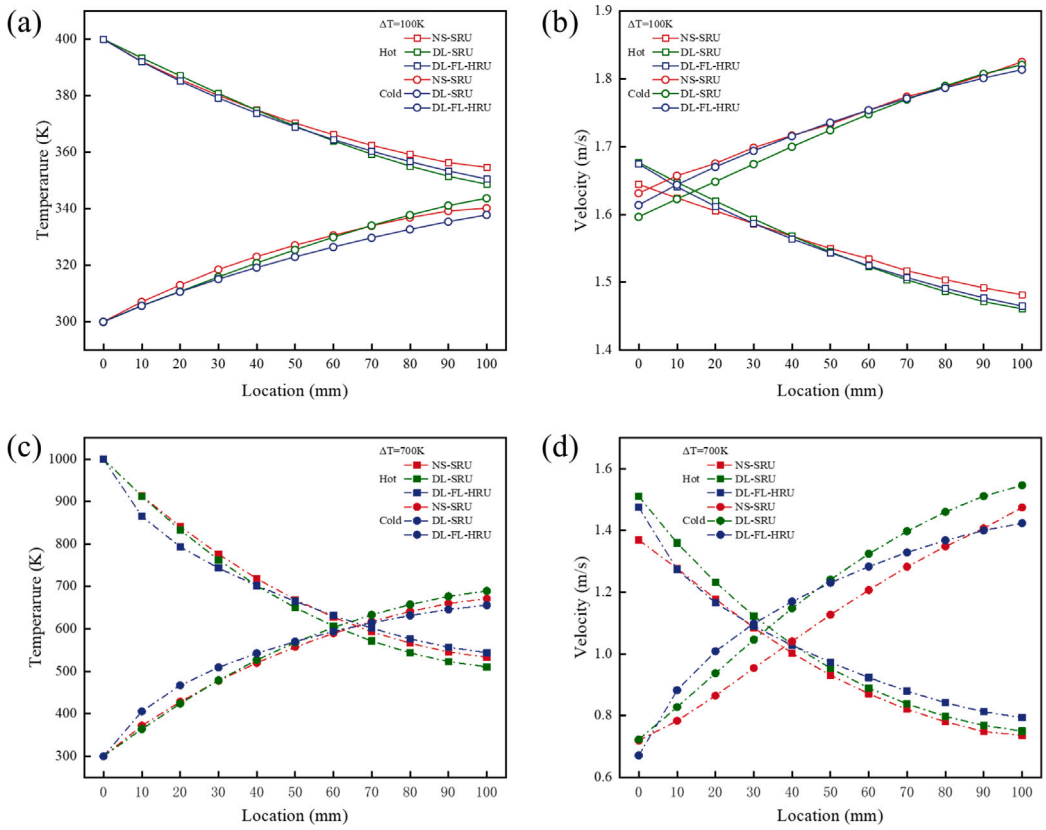


Fig. 4. Comparison of temperature and velocity of NS-SRU, DL-SRU and DL-FL-HRU model for both small (a, b) and large (c, d) temperature differences.

a deviation below 0.05%, which supports the approximation of the Navier–Stokes equations. However, compared with circular channels, square channels exhibit higher flow resistance and more non-uniform velocity distributions, which introduce additional deviations in the homogenized representation of local flow fields.

In contrast, heat transfer modeled by Fourier's law is less sensitive to geometric variation. The equivalent thermal conductivity formulation remains valid across different channel shapes, allowing consistent prediction of temperature fields. Therefore, despite geometric asymmetry, the homogenized models maintain acceptable accuracy in predicting overall thermo-fluid performance.

4.1.3. Application to multi-layer stacked structure

The proposed modeling approaches are extended to a five-layer staggered-flow plate heat exchanger, denoted as NS-MRU, DL-MRU, and DL-FL-HMRU. The detailed distributions of temperature and velocity predicted by the three models are shown in Fig. 6(a)–(f), with cross-sectional average profiles in Fig. 6(g)–(h).

Both homogenized models reproduce the temperature evolution along the flow direction for hot and cold streams. The DL-MRU model agrees well with the NS-MRU results, with temperature deviations within ±4%. The DL-FL-HMRU model shows slightly larger deviations, generally within 6.0%, mainly in regions with strong temperature gradients. Despite these local differences, the global temperature distribution and interlayer heat transfer are captured consistently. A similar behavior is observed for the velocity field. The DL-MRU model remains close to the NS-MRU results, with most deviations within ±10%. The DL-FL-HMRU model shows larger deviations in limited regions, especially where density variation and flow redistribution are significant. The maximum velocity difference remains below 0.13 m/s. The overall evolution of velocity along the flow direction is preserved.

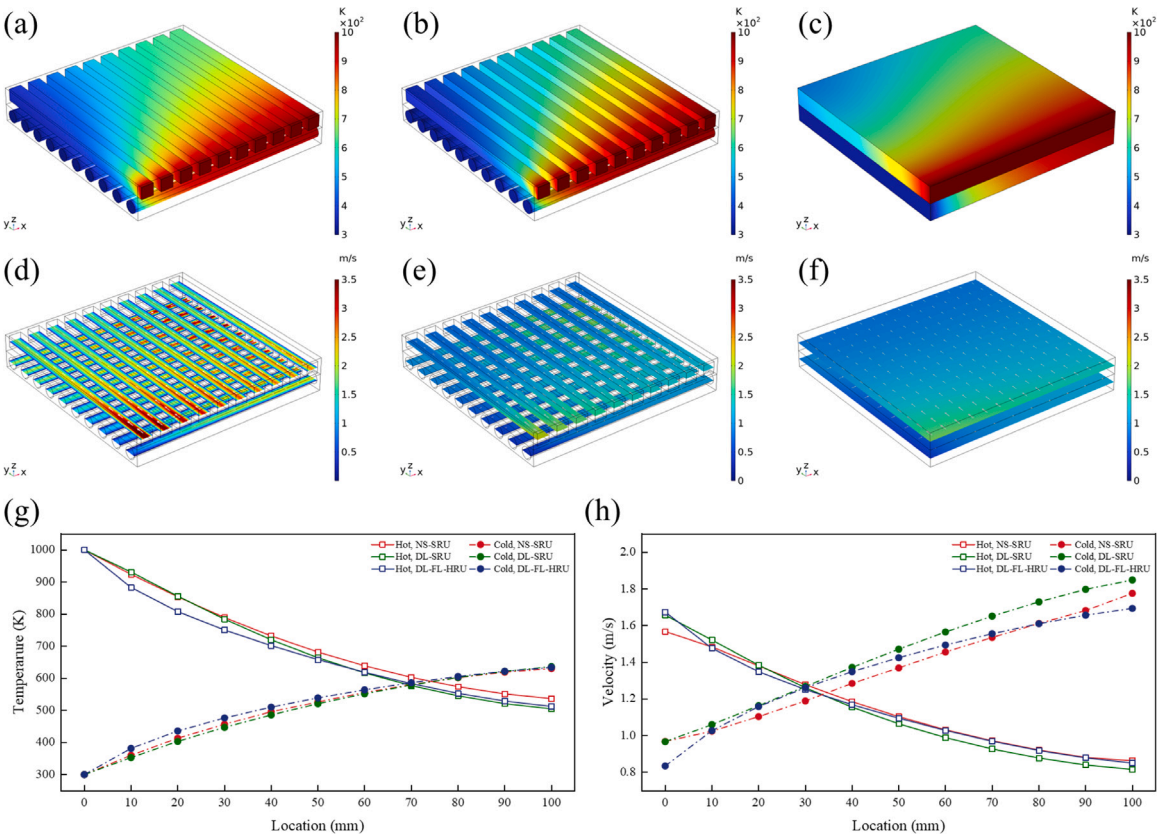


Fig. 5. Comparison of temperature and velocity NS-SRU model, DL-SRU model and DL-FL-HRU model for square–circular channel heat exchanger: (a)–(c) temperature distributions; (d)–(f) velocity distributions; (g) cross-sectional average temperature; (h) cross-sectional average velocity.

The deviations originate from enhanced coupling between flow and heat transfer in the multi-layer configuration. Multiple interfaces and strong temperature gradients lead to larger variations in fluid properties, which increase local discrepancies. These deviations remain confined and do not affect the overall transport behavior.

Compared with the single-layer configuration, the multi-layer extension does not lead to significant error accumulation. The homogenized models maintain consistent predictive capability across scales and capture interlayer interactions. This indicates that the proposed approach provides a reliable balance between accuracy and computational efficiency for multi-layer compact heat exchangers.

4.2. Variable cross-section plate heat exchangers

4.2.1. Homogenization of variable cross-section channel repeating units

For the 20-channel plate heat exchanger unit, the cold inlet temperature is fixed at 300 K, while the hot inlet temperature varies from 500 K to 1000 K. The homogenized model is compared with the N–S model using the average cold velocity, average hot velocity, and overall average temperature as evaluation metrics. The results are shown in Fig. 7.

For the single-layer arrangement, as shown in Fig. 7(a), the homogenized model agrees well with the N–S model, with relative deviations within ±2.5% over the entire operating range. The deviations show slight variation with increasing hot inlet temperature but remain small. At higher temperatures, local discrepancies increase due to stronger coupling between flow and heat transfer and property variation, while the overall prediction remains stable. This indicates that the homogenization approach captures the dominant transport behavior for geometrically regular channel structures.

For the cross-layered arrangement shown in Fig. 7(b), the channel cross section varies along the flow direction. Therefore, a piecewise permeability function is introduced to represent the spatial variation in flow resistance. Two permeability values, κ_1 and κ_2, are assigned to the corresponding local channel geometries:

$$\kappa_p(x) = \begin{cases} \kappa_1, & x \in \Omega_1, \\ \kappa_2, & x \in \Omega_2. \end{cases} \tag{27}$$

Here, Ω_1 and Ω_2 denote the unions of the intervals corresponding to the two geometrical regions. Their boundaries are determined directly from the dimensions and locations of the original channel structure. The computational mesh is locally refined near the permeability-transition interfaces. For the cross-layered configuration, the principal direction of the permeability tensor is aligned with the local channel direction in each layer.

The deviations in both cold and hot average velocities remain within 2%, and the overall temperature deviation is within 3%. These results indicate that the homogenized model maintains high accuracy for variable cross-section channels.

Compared with the single-layer arrangement, slightly larger deviations are observed in the cross-layered configuration due to enhanced pressure variation and flow redistribution. However, the deviations remain limited, indicating that the spatial permeability representation captures the influence of variable cross-section geometry on the overall flow behavior. This result demonstrates the capability of the homogenized model to handle spatially varying flow resistance in complex channel geometries.

4.2.2. Applications to variable cross-section stacked structures

Stacked plate heat exchanger models with five repeating units are constructed for two configurations using the N–S model and the homogenized approach. The models are compared using the average velocities of the cold and hot fluids and the overall average temperature.

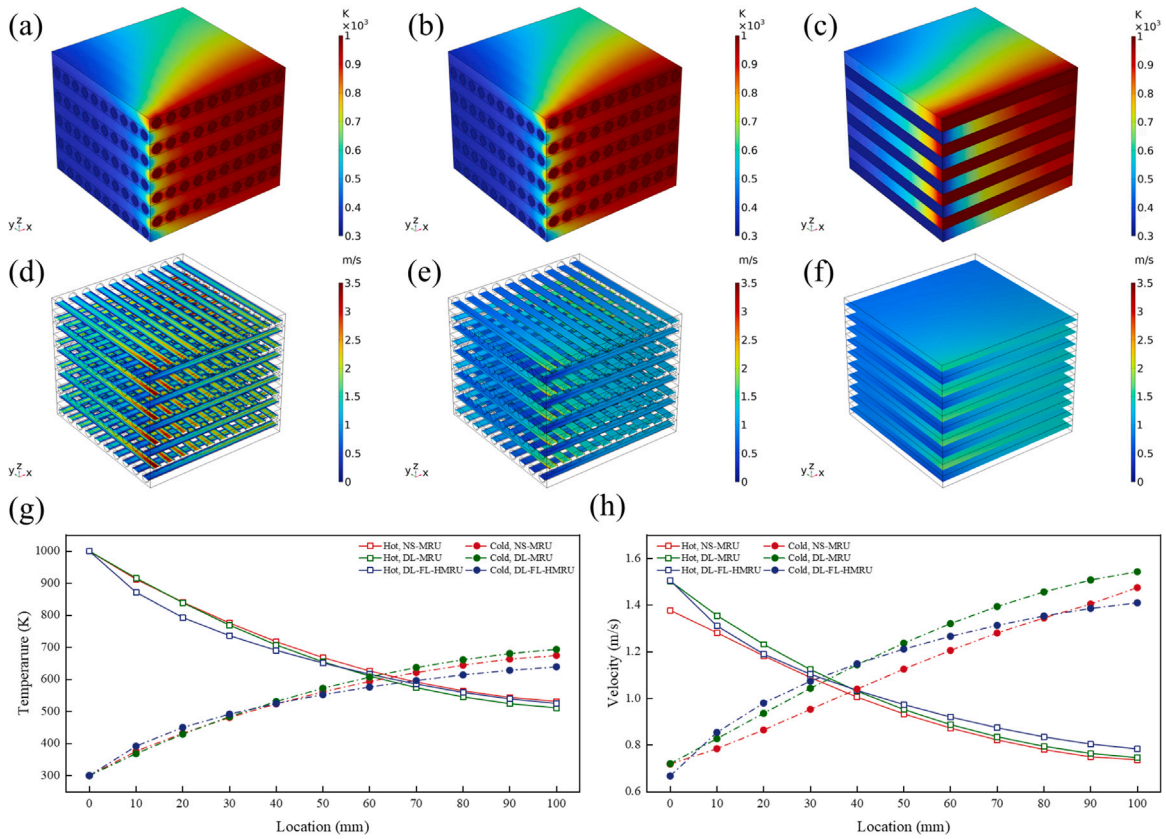


Fig. 6. Comparison of velocity and temperature of NS-MRU model, DL-MRU model and DL-FL-HMRU model for a five-layer plate heat exchanger: (a)–(c) temperature distributions; (d)–(f) velocity distributions; (g) cross-sectional average temperature; (h) cross-sectional average velocity.

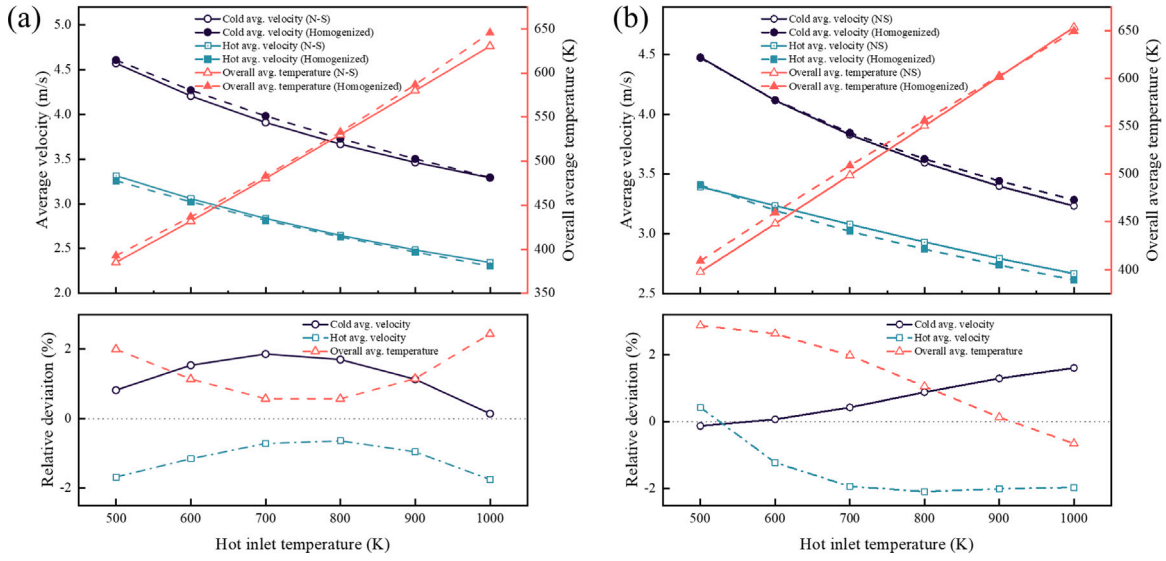


Fig. 7. Velocity and temperature comparison of single-layer and cross-layered PHE unit: (a) single-layer arrangement; (b) cross-layered arrangement.

The 3D temperature fields of the cross-layered stacked structure predicted by the two models are shown in Fig. 8(a)–(b). The homogenized model reproduces the global temperature distribution of the N–S model and captures the streamwise temperature gradient and interlayer heat transfer.

For the single-layer stacked structure, the homogenized model agrees well with the N–S model. As shown in Fig. 8(c), the relative deviation of the average cold-side velocity ranges from 1.4% to 3.8%, and that of the hot-side velocity ranges from −1.1% to 1.6%. The overall average temperature deviation ranges from −2.4% to 1.4%, indicating a slight underestimation at high temperatures. All deviations remain within ±4%. No accumulation of deviations is observed in the five-layer structure, which indicates stable performance across layers.

For the cross-layered stacked structure, the homogenized model also captures the overall trends, with increased deviations. As shown in Fig. 8(d), the deviation of the average cold-side velocity ranges from 2.7% to 4.5%, and that of the hot-side velocity ranges from −3.2% to 1.9%. The overall temperature deviation ranges from −3.5% to

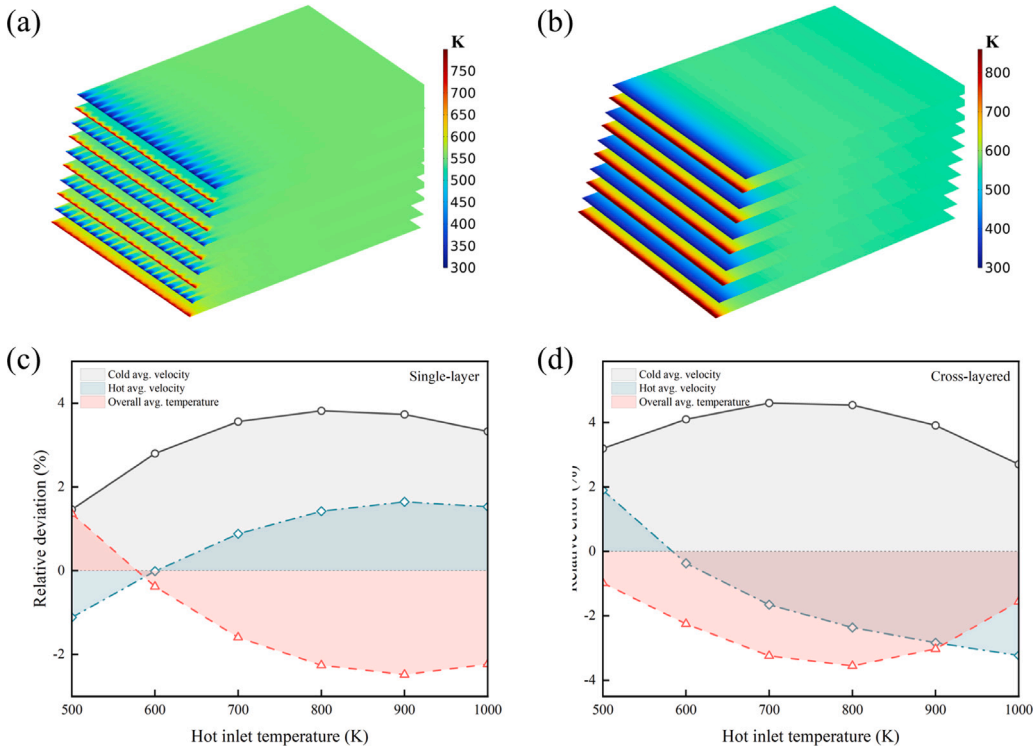


Fig. 8. Comparison of temperature distributions and prediction deviations for single-layer and cross-layered configurations: (a) single-layer temperature distribution; (b) cross-layered temperature distribution; (c) single-layer deviation; (d) cross-layered deviation.

−1.0%, indicating consistent underestimation. All deviations remain within approximately ±5%, which shows that the homogenized model with piecewise permeability represents the macroscopic thermo-fluid behavior.

Compared with the single-layer configuration, the larger deviations in the cross-layered structure result from increased geometric complexity. This enhances interlayer coupling, flow redistribution, and pressure variation, which increases the difficulty of resolving local features. However, the deviations remain limited, indicating that the homogenized approach is robust for multi-layer variable cross-section systems.

4.2.3. Performance comparison of PHE configurations using the homogenized model

Under identical boundary conditions, the heat transfer performance of single-layer and cross-layered configurations is evaluated using the homogenized model. The heat transfer rate as a function of Reynolds number is used to assess the effect of structural design for both unit and stacked models.

For the repeating-unit model, as shown in Fig. 9, the heat-transfer rate increases with decreasing Reynolds number for both configurations. The cross-layered configuration consistently achieves a higher heat-transfer rate, with an enhancement of approximately 50%–60%. This improvement arises from the combined effects of increased residence time, flow redistribution, and thermal boundary-layer redevelopment. The lower flow velocity extends the fluid residence time, allowing the fluid temperature to approach the solid temperature more closely. The spatial variation in hydraulic resistance redistributes the flow among different channel regions, promoting more uniform utilization of the heat-transfer area. In addition, repeated changes in the local cross section and flow direction interrupt the continuous development of the thermal boundary layer, thereby renewing the fluid–solid temperature gradient and enhancing convective heat transfer. A similar trend is observed for the stacked model, with stronger

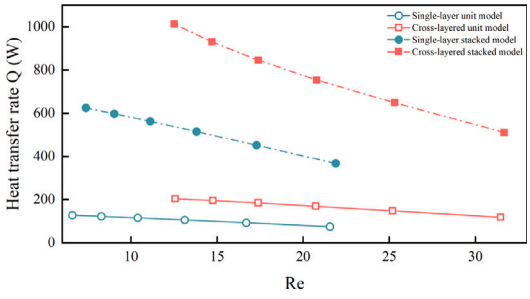


Fig. 9. Heat transfer performance comparison of single-layer and cross-layered configurations.

enhancement. The performance gain increases from about 40% to over 60%, particularly at low Reynolds numbers, indicating that the combined effects of residence time, flow redistribution, and repeated thermal boundary-layer redevelopment become more pronounced in the stacked configuration.

The homogenized model is intended to predict macroscopic temperature, velocity, and flow-distribution characteristics rather than channel-scale details. Therefore, thermal boundary-layer redevelopment, local separation, recirculation, and near-wall gradients are not explicitly resolved; their macroscopic effects are represented through the geometry-dependent permeability and anisotropic effective transport properties. The model may consequently lose accuracy in entrance regions, near abrupt geometric transitions, or at higher Reynolds numbers where inertial and secondary-flow effects become significant.

Overall, the cross-layered configuration improves heat transfer performance, and the homogenized model captures these differences with low computational cost. This supports its use for rapid performance evaluation and structural optimization of heat exchanger designs.

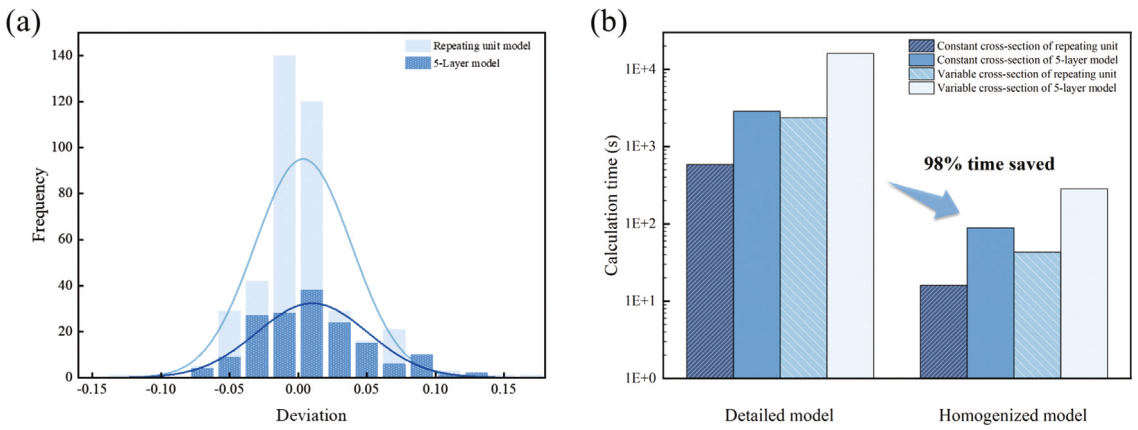


Fig. 10. Statistical distribution of prediction deviations and comparison of computational efficiency: (a) prediction deviation distribution; (b) computational efficiency comparison.

4.3. Accuracy and computational efficiency of the homogenized models

The prediction accuracy and computational efficiency of the homogenized models for both repeating unit and five-layer stacked configurations are summarized in Fig. 10(a). A total of 420 deviation samples were collected for the repeating unit model and 164 samples for the stacked model, covering temperature, velocity, and pressure fields.

As shown in Fig. 10(a), the deviation distribution is approximately Gaussian and centered around zero, which indicates unbiased prediction. More than 97.7% of the samples fall within ±10%, and 74.2%–84.6% fall within ±5%. Under moderate temperature variation, the deviations of key variables remain within ±2%, which indicates high prediction accuracy.

Fig. 10(b) compares the wall-clock solution times of the three models using the same 48-core computational configuration and convergence criterion. For the single-layer configuration, the N–S, Darcy, and homogenized models required 9 min 45 s, 1 min 28 s, and 16 s, respectively. For the multi-layer configuration, the corresponding solution times were 47 min 42 s, 3 min 15 s, and 1 min 29 s. Compared with the N–S models, the homogenized models reduce computational time by 97% for both unit and stacked configurations.

In addition, the computational cost of the N–S model increases significantly with geometric complexity, particularly for cross-layered and multi-layer structures. In contrast, the homogenized model shows only a small increase in computational time, which indicates a low sensitivity to structural complexity.configurations.

Overall, the homogenized approach achieves a good balance between accuracy and computational efficiency. It maintains acceptable deviations under variable operating conditions while significantly reducing computational cost. The results demonstrate its applicability to complex geometries and large-scale configurations, supporting its use for rapid performance evaluation and system-level modeling of plate heat exchangers.

5. Conclusion

Plate heat exchangers exhibit geometric complexity and strong multiphysics coupling, which lead to high computational cost in numerical simulations. To address this issue, a 3D homogenized model is developed, in which detailed geometries are represented by an equivalent anisotropic porous medium. The flow field is described using Darcy's law, and heat transfer is represented by an equivalent anisotropic thermal conductivity tensor, while accounting for coupling effects and temperature-dependent properties. The method is applied to both cross-flow configurations with constant cross-section channels and parallel-flow configurations with variable cross-section channels. Its validity is evaluated using repeating-unit and five-layer stacked models through comparison with full-geometry Navier–Stokes simulations. The main conclusions are as follows:

- The proposed model shows consistent predictive accuracy across geometries and operating conditions. For regular channel structures, deviations remain within ±2% under moderate temperature conditions and within ±10% under large temperature differences. For variable cross-section and cross-layered configurations, deviations are within ±5%. The model captures the dominant flow and heat transfer behavior, while local discrepancies are associated with strong temperature gradients and property variation, which affect flow and heat transfer characteristics.
- The homogenized model is effective for performance evaluation of different configurations of heat exchangers. The cross-layered structure increases heat transfer by approximately 50%–60% at the unit level, with additional enhancement in stacked systems. This enhancement is associated with increased fluid residence time and the disruption of the thermal boundary layer. The extended residence time promotes heat exchange, while the periodic variation of flow direction reduces thermal boundary layer resistance.
- The homogenized model achieves a balance between accuracy and computational efficiency. Analysis of 584 samples shows that the deviation distribution is approximately Gaussian. More than 98% of the samples fall within ±10%, and most samples are concentrated within ±2%, indicating high prediction reliability. The computational time is reduced by 97% compared with the Navier–Stokes model, which enables efficient large-scale and complex simulations.

The proposed homogenization approach provides a fast and reliable tool for performance prediction and is suitable for structural comparison of plate heat exchangers with complex channel configurations. It enables efficient prediction of coupled flow and heat transfer behavior and can be extended to layered energy conversion devices, such as fuel cells and electrolyzers. The method significantly enhances the design capabilities of manufacturers and may facilitate feedback from system designers by making it easier to share results based on a simplified and highly accurate methodology.

CRediT authorship contribution statement

Xiaolu Wang: Writing – original draft, Visualization, Validation, Software, Methodology, Investigation, Conceptualization. **Shuang Zhao:** Writing – review & editing, Methodology. **Jan Van herle:**

Supervision, Methodology. **Oscar Furst:** Writing – review & editing. **Olaf Deutschmann:** Supervision, Methodology. **Xing-Yuan Miao:** Writing – review & editing, Methodology. **Yumeng Zhang:** Writing – review & editing, Methodology. **Umberto Desideri:** Writing – review & editing, Supervision, Methodology. **Ligang Wang:** Writing – review & editing, Supervision, Project administration, Methodology, Funding acquisition, Conceptualization. **Yongping Yang:** Supervision, Methodology.

Declaration of competing interest

The authors declare that they have no known competing financial interests or personal relationships that could have appeared to influence the work reported in this paper.

Acknowledgments

This work was supported by the National Natural Science Foundation of China (52276186, 52522611, 52306240). This work was also supported in part by the National Key R&D Program of China (2024YFE0207200) and the *Joint R&D on High-temperature Electrolysis*, Beijing Major Science and Technology Project under Contract No. Z251100007125026. Additionally, this work received funding from the Clean Hydrogen Partnership under Grant Agreement No. 101137866.

Appendix A. Supplementary data

Supplementary material related to this article can be found online at https://doi.org/10.1016/j.egyai.2026.100923.

Data availability

Data will be made available on request.

References

[1] Awais Muhammad, Bhuiyan Arafat A. Heat and mass transfer for compact heat exchanger (CHXs) design: A state-of-the-art review. Int J Heat Mass Transfer 2018;127:359–80.
[2] Hesselgreaves John E. Compact heat exchangers: Selection, design, and operation. Pergamon; 2001.
[3] Zhang Jian-Fei, He Ya-Ling, Tao Wen-Quan. 3D numerical simulation on shell-and-tube heat exchangers with middle-overlapped helical baffles and continuous baffles–part I: Numerical model and results of whole heat exchanger with middle-overlapped helical baffles. Int J Heat Mass Transfer 2009;52(23):5371–80.
[4] Xie Jingzhe, Li Shulei, Yan Hongbin, Xie Gongnan. Numerical analysis on thermal–hydraulic performances of staggered tube bundles for an aero-engine compact precooler. J Therm Anal Calorim 2020;141(1):387–99.
[5] Zargoushi A, Talebi F, Hosseini SH. CFD modeling of industrial cold box with plate-fin heat exchanger: Focusing on phase change phenomenon. Int J Heat Mass Transfer 2020;147:118936.
[6] Laschet Gottfried. Homogenization of the fluid flow and heat transfer in transpiration cooled multi-layer plates. J Comput Appl Math 2004;168(1):277–88.
[7] Rizvandi Omid Babaie, Miao Xing-Yuan, Frandsen Henrik Lund. Fast and stable approximation of laminar and turbulent flows in channels by Darcy's law. Alex Eng J 2021;60(2):2155–65.
[8] Zhu Qingzi, Pishahang Mehdi, Caccia Mario, Kelsall Colin C, LaPotin Alina, Sandhage Kenneth H, et al. Validation of the porous medium approximation for hydrodynamics analysis in compact heat exchangers. J Fluids Eng 2022;144(081403).
[9] Wang Weijia, Wang Fengli, Kong Yanqiang, Yang Lijun, Niu Yuguang, Du Xiaoze, et al. Anti-freezing performance and application of air-cooled heat exchanger with different water entry patterns. Appl Therm Eng 2021;182:116066.
[10] Xu Zirui, Tan Yin, Liu Dechao, Chen Wangnan, Zhang Xiaoxu, Yang Xiongwei, et al. Equivalent mechanical property calculation method of mini-channels in printed circuit heat exchanger. Nucl Eng Des 2023;412:112468.
[11] Xu Zirui, Zhang Xiaoxu, Tan Yin, Li Ri, Yang Xiongwei, Wang Qiuwang, et al. Study on a numerical homogenization method for printed circuit heat exchanger with hybrid mini-channels. Nucl Eng Des 2024;424:113252.
[12] Yang Zhipeng, He Shaopeng, Yu Jiacheng, Wang Qianglong, Qiu Hanrui, Wang Mingjun, et al. A machine learning-based generative design approach for rapid topology optimization of microchannel heat sinks. Int Commun Heat Mass Transfer 2025;169:109655.
[13] Baker MJ, Tabor GR. Computational analysis of transitional air flow through packed columns of spheres using the finite volume technique. Comput Chem Eng 2010;34(6):878–85.
[14] Yang Jie, Ma Lei, Bock Jessica, Jacobi Anthony M, Liu Wei. A comparison of four numerical modeling approaches for enhanced shell-and-tube heat exchangers with experimental validation. Appl Therm Eng 2014;65(1):369–83.
[15] Kim Jaemin, Sibilli Thierry, Ha Man Yeong, Kim Kuisoon, Yoon Sang Youl. Compound porous media model for simulation of flat top U-tube compact heat exchanger. Int J Heat Mass Transfer 2019;138:1029–41.
[16] Ding Wenhao, Eri Qitai, Kong Bo, Zhang Zhen. Numerical investigation of a compact tube heat exchanger for hypersonic pre-cooled aero-engine. Appl Therm Eng 2020;170:114977.
[17] Li Zhen-zhong, Ding Yu-dong, Liao Qiang, Cheng Min, Zhu Xun. An approach based on the porous media model for numerical simulation of 3D finned-tubes heat exchanger. Int J Heat Mass Transfer 2021;173:121226.
[18] Zeng Chunjie, Qiu Hanrui, Wang Mingjun, Guo Kailun, Zhang Jing, Tian Wenxi, et al. Development of STEAM code: A steam generator tube-level three-dimensional thermal-hydraulic analysis platform. Nucl Eng Des 2025;444:114389.
[19] Zeng Chunjie, Mu Defang, Qiu Hanrui, Wang Mingjun, Wu Ge, Tian Wenxi, et al. High-fidelity full-scale three-dimensional thermal-hydraulic characteristics analysis of the primary and secondary side in a steam generator. Int J Therm Sci 2026;224:110658.
[20] He Shaopeng, Wang Mingjun, Tian Wenxi, Qiu Suizheng, Su GH. Development of an OpenFOAM solver for numerical simulations of shell-and-tube heat exchangers based on porous media model. Appl Therm Eng 2022;210:118389.
[21] Wang Weiping, Guo Jinxing, Zhang Shuwen, Yang Jian, Ding Xianting, Zhan Xuehua. Numerical study on hydrodynamic characteristics of plate-fin heat exchanger using porous media approach. Comput Chem Eng 2014;61:30–7.
[22] Musto Marilena, Bianco Nicola, Rotondo Giuseppe, Toscano Flavio, Pezzella Giuseppe. A simplified methodology to simulate a heat exchanger in an aircraft's oil cooler by means of a porous media model. Appl Therm Eng 2016;94:836–45.
[23] Juan Du, Zhao Hai-Tao. Numerical simulation of a plate-fin heat exchanger with offset fins using porous media approach. Heat Mass Transf 2018;54(3):745–55.
[24] Haider Patrick, Freko Pascal, Acher Thomas, Rehfeldt Sebastian, Klein Harald. A transient three-dimensional model for thermo-fluid simulation of cryogenic plate-fin heat exchangers. Appl Therm Eng 2020;180:115791.
[25] Haider Patrick, Freko Pascal, Acher Thomas, Rehfeldt Sebastian, Klein Harald. Influence of inlet configuration and distributor geometry on the performance of cryogenic plate-fin heat exchangers. Appl Therm Eng 2021;195:117197.
[26] Miao Xing-Yuan, Rizvandi Omid Babaie, Navasa Maria, Frandsen Henrik Lund. Modelling of local mechanical failures in solid oxide cell stacks. Appl Energy 2021;293:116901.
[27] Babaie Rizvandi Omid, Miao Xing-Yuan, Frandsen Henrik Lund. Multiscale modeling of degradation of full solid oxide fuel cell stacks. Int J Hydrog Energy 2021;46(54):27709–30.
[28] Miao Xing-Yuan, Pirou Stéven, Frandsen Henrik Lund. Mitigating distortions during debinding of a monolithic solid oxide fuel cell stack using a multiscale, multiphysics model. J Eur Ceram Soc 2022.
[29] Chi Yingtian, Lin Jin, Li Peiyang, Song Yonghua. Investigating the performance of a solid oxide electrolyzer multi-stack module with a multiphysics homogenized model. J Power Sources 2024;594:234019.
[30] Wang Zhongyi, Wang Ruihao, Li Zheng, Wang Meng, Wan Lei. Numerical investigation on the effect of cylindrical turbulator on performance of corrugated plate-fin heat exchanger. Appl Therm Eng 2023;230:120726.
[31] Navasa Maria, Miao Xing-Yuan, Frandsen Henrik Lund. A fully-homogenized multiphysics model for a reversible solid oxide cell stack. Int J Hydrog Energy 2019;44(41):23330–47.
[32] Shah RK, London AL. Chapter VII- Rectangular ducts. In: Shah RK, London AL, editors. Laminar flow forced convection in ducts. Academic Press; 1978, p. 196–222.
[33] Incropera FP, DeWitt DP, Bergman TL, Lavine AS. Fundamentals of heat and mass transfer. 7th ed. John Wiley & Sons; 1999.
[34] Daun KJ, Beale SB, Liu F, Smallwood GJ. Radiation heat transfer in planar SOFC electrolytes. J Power Sources 2006;157(1):302–10.
[35] Jahan Salma, Nasrin Rehena. Role of physical structure on performance index of crossflow microchannel heat exchanger with regression analysis. Adv Model Simul Eng Sci 2024;11(1):17.
[36] Jahan Salma, Nasrin R, Biswas Chaity, Zannatul Ferdoushi Most. Sensitivity study for performance evaluation criterion of a crossflow microchannel heat exchanger using response surface model. Int J Ambient Energy 2025;46(1):2507142.
[37] Jahan Salma, Nasrin Rehena. Sensitivity study of thermal enhancement featuring ternary-hybrid nanofluid in a two-layered cross-flow microchannel heat exchanger. J Therm Anal Calorim 2025;150(21):17591–616.

[38] Al-Zahrani Salman, Islam Mohammad S, Saha Suvash C. Comparison of flow resistance and port maldistribution between novel and conventional plate heat exchangers. Int Commun Heat Mass Transfer 2021;123:105200.
[39] Kong Fulin, Wang Xiaoxiao, Guo Wei, Li Xiaoyu, Ren Yongqiang, Xu Shisen. Effects of key thermal parameters on the flow boiling process of water and prediction of the heat transfer coefficient in the corrugated plate heat exchanger. Int Commun Heat Mass Transfer 2025;163:108709.
[40] Kong Fulin, Wang Xiaoxiao, Guo Wei, Li Xiaoyu, Ren Yongqiang, Xu Shisen. Effects of key structural parameters on the flow boiling process of water in the corrugated plate heat exchanger. Int Commun Heat Mass Transfer 2025;167:109364.
[41] Zong Jiezheng, Zhang Lili, Liang Xiaofu, Zhang Yongliang, Zhang Yu-Wei, Nie Zhikun, et al. Numerical simulation of plate-fin heat exchanger and design of novel turbulator structures using a multi-scale simulation approach. Int Commun Heat Mass Transfer 2025;164:108897.
[42] Gut Jorge AW, Pinto José M. Modeling of plate heat exchangers with generalized configurations. Int J Heat Mass Transfer 2003.
[43] Gut Jorge AW, Pinto José M. Optimal configuration design for plate heat exchangers. Int J Heat Mass Transfer 2004;47(22):4833–48.
[44] Galeazzo Flavio CC, Miura Raquel Y, Gut Jorge AW, Tadini Carmen C. Experimental and numerical heat transfer in a plate heat exchanger. Chem Eng Sci 2006;61(21):7133–8.